Research Square

Preprints are preliminary reports that have not undergone peer review.
They should not be considered conclusive, used to inform clinical practice,
or referenced by the media as validated information.

Evaluating the Traditional Substitutability of Hemidesmus indicus and Decalepis hamiltonii: A Comparative In-Silico Anti- Inflammatory Study

Manisha Rao
Yenepoya University
Reshma Shettigar
dr.reshmayamch@yenepoya.edu.in

Yenepoya University

Article

Keywords: Hemidesmus indicus, Decalepis hamiltonii, Molecular Docking, Redocking Validation, Caspase-1, JAK-1, COX-2

Posted Date: November 18th, 2026

DOI: https://doi.org/10.21203/rs.3.rs-11168969/v1

License: This work is licensed under a Creative Commons Attribution 4.0 International License.
Read Full License

Additional Declarations: No competing interests reported.

Evaluating the Traditional Substitutability of *Hemidesmus indicus* and *Decalepis hamiltonii*: A Comparative *In-Silico* Anti-Inflammatory Study

Manisha Rao [1], ***Reshma Shettigar****

[1,*] *Yenepoya Ayurveda Medical College and Hospital, Yenepoya Deemed to Be University.*

***Corresponding author:** **Reshma Shettigar** dr.reshmayamch@yenepoya.edu.in

Abstract

Hemidesmus indicus (HI) and *Decalepis hamiltonii* (DH), are both members of the Apocyanaceae family, and are traditionally used as coolants, blood purifiers, and anti-inflammatory agents. They are often used in place for one another due to their overlapping ethnobotanical applications and similar chemical profiles. Therefore, the present study had two objectives; to phytochemically profile HI and DH using LC-MS, and to evaluate the anti-inflammatory potential of the identified phytocompounds through in silico molecular docking and ADMET profiling. Both the plant extracts were obtained, phytocompounds were classified into major chemical groups and tested against the important inflammatory targets related to skin inflammatory processes such as: Caspase-1 (PDB ID: 6F6R), JAK-1 (PDB ID: 6N77) and COX-2 (PDB ID: 5IKR). The RMSD value obtained for co-crystallized ligands of Caspase-1 (6F6R), JAK-1 (6N77) and COX-2 (5IKR) was 0.0 Å which indicated that the docking workflow was accepted. Results of molecular docking indicated that the phytocompounds possessed several non-covalent interactions and showed mean higher binding affinities in both the species, although some metabolites were unique to HI which showed comparatively higher binding affinities and non-covalent interactions, compared to those detected in DH. The comparative analysis illustrated that HI has a few common phytocompounds, supporting its interchangeability with the other species, but the HI exhibited much wider spectrum bioactive metabolites which can act on various inflammatory symptoms of the pathways. In general, DH and HI had similar predicted multi-target anti-inflammatory interactions with HI having stronger interactions. Our results provide a view of the molecular cause underlying their traditional use and hints on their level of substitutions; although the latter requires some more experimental confirmations in the future.

Keywords: *Hemidesmus indicus; Decalepis hamiltonii;* Molecular Docking; Redocking Validation; Caspase-1; JAK-1; COX-2

1. Introduction

Hemidesmus indicus (L.) R. Br. (HI), commonly known as Indian sarsaparilla, and *Decalepis hamiltonii Wight & Arn. (DH),* referred to as Swallow root, possess aromatic roots and are recognized in traditional medicine for their therapeutic properties. Both HI and DH demonstrate anti-inflammatory, antioxidant, antimicrobial, and immunomodulatory activities, as evidenced by traditional applications and experimental studies (Anusha et al., 2023; Mishra et al., 2025; Nazar et al., 2024; Sarkar & Ghosh, 2024). Traditionally, HI has been used to treat rheumatism, leprosy, impotence, urinary tract infections, and skin infections (Das, S., & Singh Bisht, S., 2013). The anti-inflammatory properties of HI have been demonstrated in a carrageenan-induced paw edema model, with efficacy comparable to diclofenac sodium (Pathan, J. K., 2018). Root decoctions of HI also exhibit dose-dependent antinociceptive effects (Sahu, P. K. (2020), which supports its traditional medicinal use. DH is recognized for its blood-purifying, antipyretic, and gastroprotective activities (Nazar et al., 2024; Sarkar & Ghosh, 2024). DH phytocompounds inhibit infectious pathogens and modulate inflammatory markers by down-regulating TNF-alpha and IL-2 and up-regulating IL-10 in vitro (Lakshman, K. (2006)). Isolated 2H4MB and long-chain lupeol esters from DH promote cell migration and facilitate wound healing (Kulatunge, D. R., 2025). Additionally, DH demonstrates antiulcer effects through antioxidant activity and increased gastric mucin secretion (Naik, Y., 2007).

The anti-inflammatory effects of HI and DH are mediated by various phytocompounds that modulate key proteins in the skin's inflammatory response, including Caspase-1, COX-2, and JAK1 (Ren et al., 2024). Caspase-1 mediates the production of pro-inflammatory cytokines. COX-2 catalyzes the synthesis of prostaglandins, which contribute to vasodilation, edema, and pain. JAK1 transduces cytokine-dependent signaling involved in chronic inflammatory and autoimmune skin diseases. These proteins are functionally interconnected and serve as important therapeutic targets for the management of inflammatory skin conditions (Adendla, E. K., (2025).

DH is often substituted for HI in Indian traditional medicine, a practice partially supported by chromatographic analyses (Aswathanarayan, J. B. (2022), Kharat, T. D., (2021), though comprehensive evidence of full therapeutic equivalence remains lacking. To address this gap, we employed molecular docking to predict the binding interactions of major phytochemicals with key inflammatory targets mediating skin infections. This computational approach provides a rational framework for evaluating their substitutability and reveals multitarget effects that warrant future experimental validation.

2. Materials and methods

2.1 Plant material and authentication

Dried roots of Decalepis hamiltonii and Hemidesmus indicus were procured from SDM Ayurveda Pharmacy, Udupi, Karnataka, a GMP-certified manufacturer, as raw drugs supplied under the trade name “Sariva”: Decalepis hamiltonii (batch 6A31CAM; Certificate of Analysis RM260106) and Hemidesmus indicus (batch 6C03LPU; Certificate of Analysis RM260185). Species identity was declared by the suppliers (Chethan Ayurved & KMC Biotech), and the material was evaluated by the manufacturer’s quality control department against pharmacopoeial quality parameters (appearance, foreign matter, ash and extractive values). The original geographic source, and whether the material was wild-harvested or cultivated, could not be established. The samples were taxonomically authenticated by Dr. Keshava Chandra, department of Botany, Excellent PU College, Mangalore, India, by organoleptic evaluation. No voucher specimens were retained, as the material consisted of dried, cut root pieces lacking the leaves, flowers, and fruits required for a herbarium specimen, and the purchased quantity was consumed during extraction and LC-MS/MS analysis. As the materials were obtained commercially, no collection permits were required and no collection from wild populations was undertaken by the authors. The study complied with relevant institutional, national, and international guidelines and legislation, and with the IUCN Policy Statement on Research Involving Species at Risk of Extinction. According to the IUCN Red List (accessed 23 October 2026), D. hamiltonii is assessed as Endangered (EN A2cd; last assessed 16 July 2014),whereas H. indicus has not been evaluated. Neither species is listed in the CITES Appendices (Checklist of CITES species, accessed 23 October 2026).

2.2 Extraction and LC-MS/MS analysis

Methanolic extracts of both plants were prepared by Soxhlet extraction, using plant:solvent ratio, for 24–48 hours, followed by filtration and concentration, and analysed by liquid chromatography-tandem mass spectrometry (LC-MS/MS) using a Xevo G2-XS QT of mass spectrometer coupled with an ACQUITY UPLC H-Class PLUS Bio System (Waters Corporation, USA) under the following conditions: ACQUITY UPLC® BEH C18 column (1.7 µm), mobile phase A (water + 0.1% formic acid) and mobile phase B (acetonitrile + 0.1% formic acid), binary gradient elution, injection volume of 0.10 µL, column temperature of 45 °C, sample tray temperature of approximately 15.2 °C, and electrospray ionisation (ESI) in positive-ion mode. The Waters Traditional Medicine Library was used for compound comparison and tentative identification.

2.3. Molecular Docking Studies: Target Protein and Ligand Optimization

To verify the reliability and reproducibility of the molecular docking method, co-crystallized ligands and their respective proteins (Caspase-1: 6F6R, JAK-1: 6N77 and Cox-2: 5IKR) have been considered. Removal of native ligands from each crystal structure followed by subsequent docking of each in each

active site, using the same docking parameters as employed for the screening of phytocompounds using AutoDock Vina.

For the docking accuracy, we compared the pose of the docked ligand to the crystallographically, experimentally determined pose. Root-mean-square deviations (RMSDs) between the native and the redocked pose were computed and deviations lower than 2.0 Å were taken as a good criterion for the reproduction of the experimental binding mode. The conformations of all three ligands obtained during the redocking procedure matched well with the crystallographic ones with the RMSD 0.0Å. The results gave binding energies of the ligand in the Caspase-1 co-crystallized structure of −3.6 kcal/mol, binding energies of the inhibitor in the JAK-1 co-crystallized structure of −8.5 kcal/mol as well as binding energies of the mefenamic acid in the COX-2 co-crystallized structure of −8.6 kcal/mol. These results provide a look into the efficacy of selected docking parameter, active-site definition and scoring function for further docking analyses towards phytocompounds.

Table 1. *Validation of the molecular docking protocol through redocking of co-crystallized ligands.*

Protein Target	PDB ID	RMSD (Å)	Binding Energy (kcal/mol)
Caspase-1	6F6R	0.0	-3.6
JAK-1	6N77	0.0	-8.5
COX-2	5IKR	0.0	-8.6

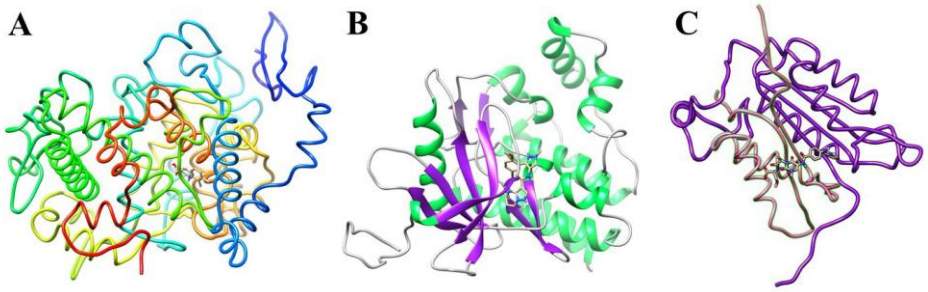


Figure 1: *Validation of docking protocol by redocking of co-crystallized ligands showing RMSD values of 0.0 Å for all targets: A) 5IKR with Mefenamic Acid, B) 6N77 with N-[3-(5-chloro-2-methoxyphenyl)-1-methyl-1H-pyrazol-4-yl]pyrazolo , C) 6F6R with N-[3-(5-chloro-2-methoxyphenyl)-1-methyl-1H-pyrazol-4-yl]pyrazolo[1,5-a]pyrimidine-3-carboxamide.*

The RMSD of 0.0 Å of the docked molecules of the complexes obtained after repositioning the molecules from the crystallographic water-ligand form in their native ligand binding conformation confirms the reliability of the docking protocol and validates the protein-ligand contacts derived in the present work.

Molecular docking simulations were performed using Pyryx integrated with the AutoDock Vina docking engine. The three-dimensional structure of human caspase-1 (PDB ID: 6F6R), COX - 2 (PDB ID: 5IKR) and JAK 1 (PDB ID: 6N77) was obtained from the Protein Data Bank. The protein structures were prepared by removing water molecules, adding polar hydrogen atoms, and assigning Gasteiger

partial charges using UCSF Chimera. Ligand structures were prepared and energy-minimized using UCSF Chimera prior to docking, followed by assignment of Gasteiger charges and conversion to PDBQT format, with Gasteiger charges assigned for all atoms.

The docking search space was defined around one of the active-site residues of each of the target proteins, as revealed by both co-crystallized ligand and as reported in the literature. The exhaustiveness parameter was set to 32 and 9 binding poses were found for each ligand for a good conformational sampling. The AutoDock Vina scoring function was used to obtain the values of binding affinities that are reported as binding free energies (kcal/mol). The inhibition constant (Ki) was calculated from the aforementioned equations by using the universal gas constant value (R) of 1.987 cal mol^{-1} K^{-1} and the absolute temperature (T) of 298.15 K, which is the temperature used in the experiment. The docking protocol was further checked by re-docking the co-crystallized drugs and validation of the results by comparing to the experimental drug-protein structures provided in the PDB, with an RMSD of 0.0 Å obtained for all the target proteins.

2.2 Interaction Analysis

Protein-ligand interactions were analyzed using the Protein-Ligand Interaction Profiler (PLIP) web service (https://plip-tool.biotec.tu-dresden.de/). The top-ranked docking pose was submitted to PLIP for automated detection and characterization of non-covalent interactions including hydrophobic contacts, hydrogen bonds, π-cation interactions, salt bridges, and π-stacking. Interaction distances and geometric parameters were extracted from the PLIP output for detailed analysis.

2.3 Visualization

Molecular structures and binding poses were visualized using Chimera (version 1.19). Protein structures are displayed as cartoon representations, and ligands are shown as sticks with atoms colored by element (carbon: cyan/yellow, oxygen: red, nitrogen: blue). Interaction distances are indicated by dashed lines color-coded by interaction type (hydrophobic: brown, hydrogen bonds: blue, π-cation: orange).

2.4 In Silico ADMET Prediction Analysis

The in silico computational tools used for drug designing and screening the new drug for the prediction of pharmacokinetic (absorption, distribution, metabolism, and excretion; ADME) and toxicity profiles. For these purposes, the following phytocompounds were selected: 2-hydroxy-4-methoxybenzaldehyde, borneol, β-sitosterol, ellagic acid, kaempferol, quercetin, and β-amyrin, and their canonical Simplified Molecular Input Line Entry System (SMILES) notation was retrieved from the PubChem database (https://pubchem.ncbi.nlm.nih.gov/) and used as the input structure for all predictions. To investigate the DH and HI derivatives, ADMET properties were predicted using the pkCSM online server (http://biosig.unimelb.edu.au/pkcsm/) and cross-verified with the SwissADME web tool (http://www.swissadme.ch/). The predicted values for the absorption (water solubility, human

intestinal absorption, skin permeability and P-glycoprotein substrate status), distribution (steady-state volume of distribution and blood–brain barrier permeability), metabolism (cytochrome P450 substrate and inhibitor status), excretion (total clearance and renal organic cation transporter 2 [OCT2] substrate status) and toxicity (AMES mutagenicity, maximum tolerated dose, oral rat acute and chronic toxicity, hepatotoxicity and skin sensitisation) endpoints were recorded.

3. Results

3.1 LCMS analysis

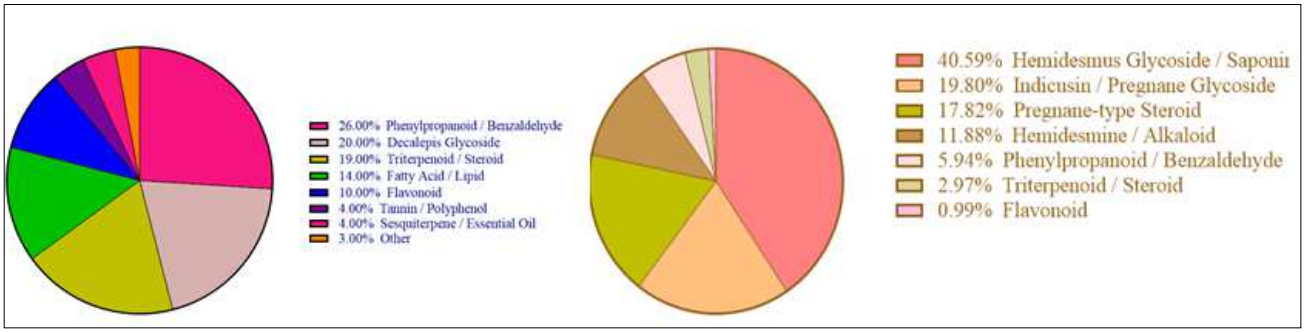


Figure 2: *Class distribution of different phytocompounds from DH (Figure 1A) and HI (Figure 1B).*

The LC-MS/MS analysis of DH and HI revealed distinct phytochemical class distributions in both species (Figure 2). In DH (Figure 1A), phenylpropanoid constituted the major class accounting for 26.00% of the total identified compounds, followed by Decalepis Glycoside (20.00%), Triterpenoid/Steroid (19.00%), Fatty Acid/Lipid (14.00%), and Flavonoid (10.00%). In HI (Figure 1B), Hemidesmus Glycoside/Saponin was the dominant class (40.59%), followed by Indicusin/Pregnane Glycoside (19.80%), Pregnane-type Steroid (17.82%), and Hemidesmine/Alkaloid (11.88%). Comparative analysis showed that Phenylpropanoid, Triterpenoid/Steroid, and Flavonoid classes were shared between both species, with DH exhibiting a higher Phenylpropanoid proportion (26.00% vs. 5.94% in HI). The remaining classes were species-specific: Decalepis Glycoside, Fatty Acid/Lipid, Tannin/Polyphenol, and Sesquiterpene/Essential Oil were unique to DH, while Hemidesmus Glycoside/Saponin, Indicusin/Pregnane Glycoside, Pregnane-type Steroid, and Hemidesmine/Alkaloid were exclusive to HI, consistent with previously reported phytochemical differentiation between the two species (Thatipelli Sujith et al., 2021).

3.2 Molecular Docking Analysis

This study employed the molecular docking method to investigate interactions between ten phytocompounds from DH and HI and inflammatory proteins, including caspase-1, JAK-1, and COX-2, which play key roles in inflammatory signaling pathways, to predict their multitarget interactions. The selected phytocompounds from DH include kaempferol, β-amyrin, valline, borneol, quercetin, β-

sitosterol, and decalpin. In HI, the unique phytocompounds identified are Hemidesmus A, Hemidesmus B, heminine, quercetin 3-O-glucoside, and denicunine. Both species contain 2-hydroxy-4-methoxybenzaldehyde and lupeol derivatives, with higher concentrations in their root regions.

3.2.1 Interaction between Caspase - 1 and common phytocompounds from *DH* and *HI*

Caspase-1 is a protease with a deep S1 pocket and cysteine-histidine dyads as its active sites. During the interaction, small molecules such as HMB, B-amyrin, borneol, valine, and kaempferol have been specifically shown to interact with proteins. The other phytocompounds have lower binding affinities, indicating poor inhibitory activity. On the other hand, caspase-1, which contains Cys-285, His-237, and Arg-341 in its active sites, predominantly shows a polar nature, with nucleophilic sulfur, aromatic nitrogen, and positively charged guanidinium groups.

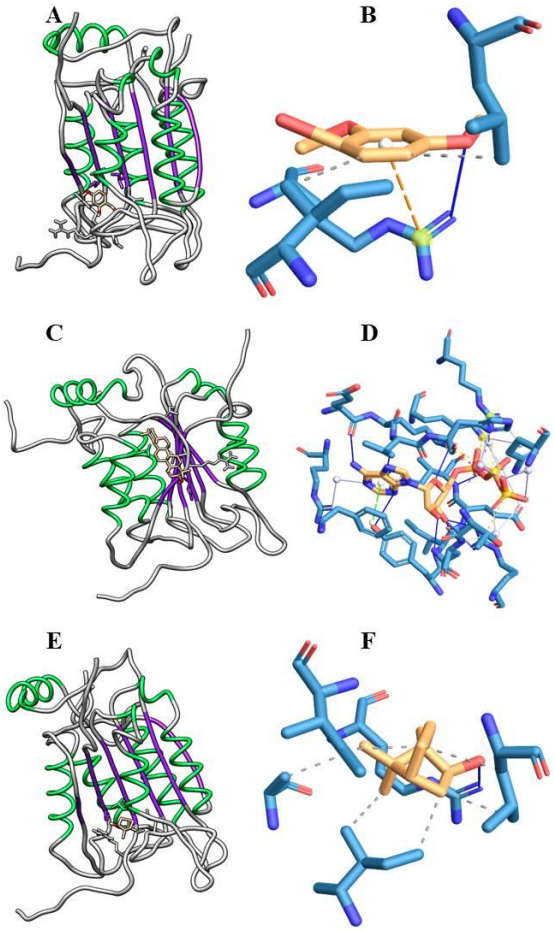


Figure 3. *Molecular docking and interaction profiles of 2-hydroxy-4-methoxybenzaldehyde (2H4MB), Beta-Amyrin, and Borneol with caspase-1. (A) 2-hydroxy-4-methoxybenzaldehyde (2H4MB) with caspase-1 (cyan cartoon). (B) 2H4MB (yellow sticks) in the binding pocket with interacting residues LEU258A, ILE282A, and ARG286A (cyan sticks). Interactions shown as dashed lines: hydrophobic (brown), H-bond (blue), π-cation (orange). Ki = 154.16 µM. (C) Beta-Amyrin with caspase-1 (green cartoon). (D) Beta-Amyrin (yellow sticks) in the binding pocket with interacting residues GLU225A, ARG226A, LYS286A, and ARG335A (cyan sticks). Interactions shown as dashed lines: hydrogen bonds (blue), salt bridge (red), π-stacking (orange), water bridges (light blue). Ki = 78.48 µM. (E) Borneol with caspase-1 (green cartoon). (F) Borneol (orange sticks) in the binding pocket with interacting residues ILE243A, LEU258A, ILE282A, ALA284A, and ARG286A (cyan sticks). Interactions shown as dashed lines: hydrophobic (brown, 6 total), hydrogen bond (blue, 1 total). Ki 92.91 µM.*

Docking analysis revealed that Beta-amyrin interacts with caspase-1, exhibiting a lowest binding affinity of -5.6 kcal/mol and a calculated inhibition constant (Ki) of 74.9 nM, which is 2,080-fold stronger than 2H4MB (Ki = 156 μM), suggesting its potential as a caspase-1 inhibitor. Protein-Ligand Interaction Profiler (PLIP) analysis identified a binding interface with 11 hydrogen bonds, 1 salt bridge, 1 π-stacking interaction, and 11 water bridges, involving approximately 15–20 caspase-1 residues. Key interacting residues include GLU225 and ARG226 (catalytic region), LYS286 and ARG335 (substrate-recognition pockets), and VAL289, ALA294, ASN389, and ASP390 (secondary binding elements). The extensive hydrogen-bonding network demonstrates strong geometric complementarity, with donor–acceptor distances of 2.5–3.5 Å and angles exceeding 170°, indicating highly directional interactions.

Docking analysis showed that Borneol binds to caspase-1 with a binding affinity of -5.5 kcal/mol and a calculated inhibition constant (Ki) of 94.3 nM. This affinity is 1,654-fold stronger than HMB (Ki = 156 μM) and slightly weaker than Beta-Amyrin (Ki = 74.9 nM), supporting its role as a secondary lead caspase-1 inhibitor. PLIP analysis identified 6 hydrophobic interactions and 1 hydrogen bond, involving 5 key residues: ILE243A, LEU258A (twice), ILE282A (twice) (hydrophobic pocket), ALA284A (stabilization), and ARG286A (hydrogen bonding). Hydrophobic contacts had van der Waals distances of 3.35–3.74 Å, indicating good packing. The hydrogen bond with ARG286A had hydrogen-acceptor and donor-acceptor distances of 2.54 Å and 3.23 Å, respectively, supporting directional specificity and electrostatic complementarity.

3.2.2 Interaction between 6N77 (JAK-1) and common phytocompounds from *DH* and *HI*

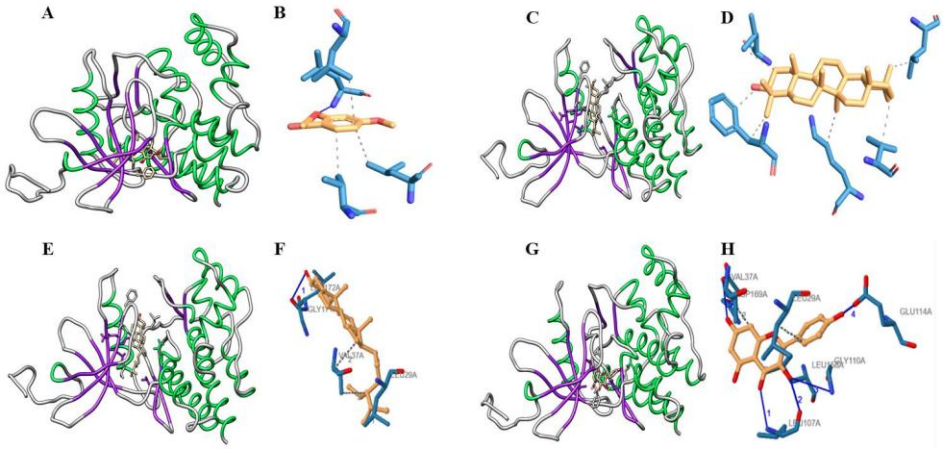


Figure 4. *Molecular docking and interaction profiles of 2-Hydroxy-4-methoxybenzaldehyde (2H4MB), β-Amyrin, β-sitosterol, and Kaempferol with JAK-1 (PDB: 6N77). (A) 2H4MB with JAK-1 (green helices, purple beta-sheets, white loops). (B) 2H4MB (orange/blue sticks) in the binding pocket with interacting residues LEU29A, VAL37A, LEU158A, and LEU107A (cyan sticks). Interactions shown as dashed lines: hydrophobic (brown, 3 total), hydrogen bond (blue, 1 total), Ki = 78.48 μM. (C) β-Amyrin with JAK-1 (green helices, purple beta-sheets, white loops). (D) β-Amyrin (orange sticks) in the binding pocket with interacting residues PHE34A, VAL37A, LYS56A, LEU158A, and LEU172A (cyan sticks). Interactions shown as dashed lines: hydrophobic (brown, 6 total), Ki = 10.22 nM. (E) β-sitosterol with JAK-1 (green helices, purple beta-sheets, white loops). (F) β-sitosterol (orange sticks) in the binding pocket with interacting residues LEU29A, VAL37A, LEU172A, and GLY171A (cyan sticks). Interactions shown as dashed lines: hydrophobic (brown, 4 total), hydrogen bond (blue, 1 total), Ki = 418.99 nM. (G) Kaempferol with JAK-1 (green helices, purple beta-sheets, white loops). (H) Kaempferol (orange sticks) in the binding pocket with interacting residues LEU29A, VAL37A, LEU158A, LEU107A, GLY110A,*

GLU114A, and ASP169A (cyan sticks). Interactions shown as dashed lines: hydrophobic (brown, 3 total), hydrogen bonds (blue, 5 total), Ki = 496.03 nM.

Docking analysis showed that 2-Hydroxy-4-methoxybenzaldehyde (2H4MB) binds to JAK-1 (PDB: 6N77) with a binding affinity of -5.6 kcal/mol and a calculated inhibition constant (Ki) of 78.48 μM. PLIP analysis identified 3 hydrophobic interactions and 1 hydrogen bond, involving 4 key residues: LEU29A, VAL37A, LEU158A (hydrophobic pocket), and LEU107A (hydrogen bonding). Hydrophobic contacts had van der Waals distances of 3.62–3.95 Å, indicating moderate packing within the binding site. The hydrogen bond with LEU107A had hydrogen-acceptor and donor-acceptor distances of 2.27 Å and 3.09 Å, respectively, with a donor angle of 139.97°, supporting electrostatic complementarity for ligand stabilization in the JAK-1 active site.

β-Amyrin binds to JAK-1 (PDB: 6N77) with a binding affinity of -10.9 kcal/mol and an inhibition constant (Ki) of 10.22 nM. Five docking poses were generated with binding affinities ranging from -10.9 to -8.0 kcal/mol, corresponding to Ki values between 10.22 nM and 1,365.70 nM. Four additional poses exhibited moderate affinity (Ki = 0.35–1.37 μM; ΔG = -8.8 to -8.0 kcal/mol) with higher RMSD values (3.71–8.41 Å).

Protein-ligand interaction analysis using PLIP identified six hydrophobic interactions involving five residues: PHE34A, VAL37A, LYS56A, LEU158A, and LEU172A. PHE34A established dual interactions at van der Waals distances of 3.61 Å and 3.52 Å. LEU158A exhibited the closest contact at 3.34 Å. VAL37A and LEU172A showed interactions at 3.71 Å and 3.73 Å, respectively. LYS56A contacted the ligand at 3.86 Å. All van der Waals distances ranged from 3.34–3.86 Å, indicating favorable geometric complementarity between the ligand and binding pocket.

β-sitosterol binds to JAK-1 (PDB: 6N77) with a binding affinity of -8.7 kcal/mol and an inhibition constant (Ki) of 418.99 nM (0.42 μM). Nine docking poses were generated with binding affinities ranging from -8.7 to -7.9 kcal/mol, corresponding to Ki values between 418.99 nM and 1,616.83 nM. The best docking pose achieved an optimal alignment with RMSD of 0.0 Å, demonstrating favorable geometric positioning within the JAK-1 binding site.

Protein-ligand interaction analysis identified four hydrophobic interactions and one hydrogen bond stabilizing the β-sitosterol-JAK1 complex. The hydrophobic interactions involve three residues: LEU29A (3.72 Å), VAL37A (dual contacts at 3.42 Å and 3.62 Å), and LEU172A (3.68 Å). These van der Waals distances fall within the optimal packing range (3.0 - 4.0 Å), indicating good geometric complementarity. A single hydrogen bond was identified with GLY171A, featuring a hydrogen-acceptor distance of 2.87 Å and a donor-acceptor distance of 3.65 Å, with a favorable donor angle of 138.39°, supporting directional specificity of the interaction. The combination of hydrophobic contacts and a hydrogen bond with β-sitosterol establishes it as a secondary JAK-1 inhibitor candidate with moderate potency suitable for further optimization and evaluation.

Kaempferol binds to JAK-1 (PDB: 6N77) with a binding affinity of -8.6 kcal/mol and an inhibition constant (Ki) of 496.03 nM (0.50 µM). Nine docking poses were generated with binding affinities ranging from -8.6 to -7.5 kcal/mol, corresponding to Ki values between 496.03 nM and 3,176.12 nM. The best docking pose achieved an alignment with RMSD of 0.0 Å. This binding affinity is 158-fold stronger than 2-Hydroxy-4-methoxybenzaldehyde (Ki = 78,478.29 nM) but weaker than β-Amyrin (Ki = 10.22 nM) and β-sitosterol (Ki = 418.99 nM).

Protein-ligand interaction analysis identified three hydrophobic interactions and five hydrogen bonds. The hydrophobic interactions involve three residues: LEU29A (3.46 Å), VAL37A (3.67 Å), and LEU158A (3.56 Å). Hydrogen bonds were formed with five residues: LEU107A (two bonds with H-A distances of 2.05 Å and 2.03 Å), GLY110A (H-A distance 3.49 Å), GLU114A (H-A distance 2.44 Å), and ASP169A (H-A distance 2.75 Å). Donor angles ranged from 112.14° to 172.57°. The combination of three hydrophobic contacts and five hydrogen bonds stabilizes the Kaempferol-JAK1 complex at the nanomolar level.

3.2.2.1 Interaction between JAK -1 and phytocompounds from HI

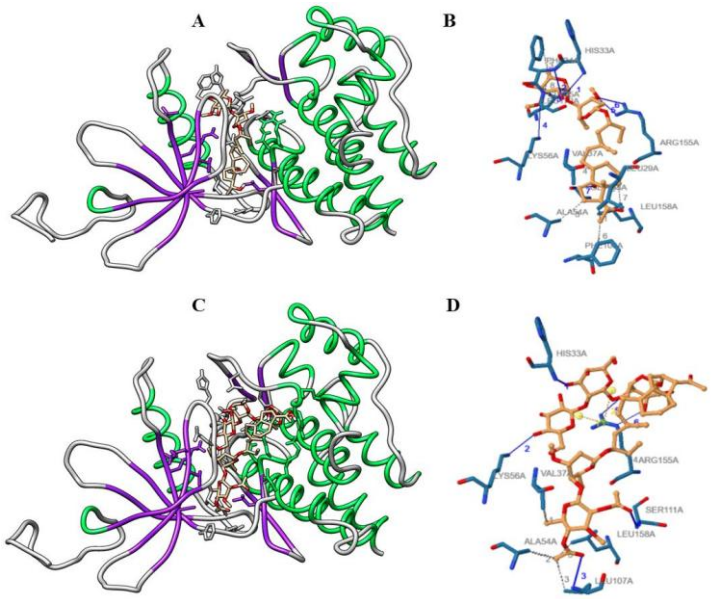


Figure 5. *Molecular docking and interaction profiles of Denicunine and Hemidesmoside A with JAK-1 (PDB: 6N77). (A) Denicunine with JAK-1 (green helices, purple β-sheets, white loops). (B) Denicunine (orange sticks) in the binding pocket with key interacting residues (blue sticks). Interactions shown as dashed lines: hydrophobic (brown, 8 total), hydrogen bonds (blue, 7 total), Ki = 46.69 nM. (C) Hemidesmoside A with JAK-1 (green helices, purple β-sheets, white loops). (D) Hemidesmoside A (orange sticks) in the binding pocket with key interacting residues (blue sticks). Interactions shown as dashed lines: hydrophobic (brown, 5 total), hydrogen bonds (blue, 6 total), salt bridges (yellow, 2 total), Ki = 298.94 nM.*

Denicunine binds to JAK-1 (PDB: 6N77) with a binding affinity of -10.0 kcal/mol and an inhibition constant (Ki) of 46.69 nM (0.05 µM). Nine docking poses were generated with binding affinities ranging from -10.0 to -9.4 kcal/mol, corresponding to Ki values between 46.69 nM and 128.54 nM. The best docking pose achieved an alignment with RMSD of 0.0 Å. This binding affinity is comparable to β-Amyrin (Ki = 10.22 nM) and 1,681-fold stronger than 2-Hydroxy-4-methoxybenzaldehyde (Ki = 78,478.29 nM). Protein-ligand interaction analysis identified eight hydrophobic interactions and seven

hydrogen bonds. The hydrophobic interactions involve eight residues: LEU29A (two interactions at 3.73 Å), PHE34A (3.92 Å), VAL37A (3.65 Å), ALA54A (3.99 Å), PHE106A (3.73 Å), LEU158A (3.11 Å), and LEU172A (3.64 Å), with distances ranging from 3.11–3.99 Å. Hydrogen bonds were formed with seven residues: HIS33A (H-A distance 3.50 Å), PHE34A (H-A distance 2.94 Å), GLY35A (H-A distance 2.46 Å), LYS56A (H-A distance 3.01 Å), ARG155A (two bonds with H-A distances of 2.22 Å and 3.21 Å), and GLY168A (H-A distance 2.37 Å). Donor angles ranged from 108.83° to 151.49°. The combination of eight hydrophobic contacts and seven hydrogen bonds establishes strong stabilization of the Denicunine-JAK1 complex at the nanomolar level.

Hemidesmoside A binds to JAK-1 (PDB: 6N77) with a binding affinity of -8.9 kcal/mol and an inhibition constant (Ki) of 298.94 nM (0.30 μM). Nine docking poses were generated with binding affinities ranging from -8.9 to -6.7 kcal/mol, corresponding to Ki values between 298.94 nM and 12,256.35 nM. The best docking pose achieved an alignment with RMSD of 0.0 Å. This binding affinity is 263-fold stronger than 2-Hydroxy-4-methoxybenzaldehyde (Ki = 78,478.29 nM) but weaker than β-Amyrin (Ki = 10.22 nM) and Denicunine (Ki = 46.69 nM). Protein-ligand interaction analysis identified five hydrophobic interactions, six hydrogen bonds, and two salt bridges. The hydrophobic interactions involve five residues: VAL37A (3.80 Å), ALA54A (3.99 Å), LEU107A (3.73 Å), ARG155A (3.16 Å), and LEU158A (3.36 Å), with distances ranging from 3.16–3.99 Å. Hydrogen bonds were formed with six residues: HIS33A (H-A distance 1.93 Å), LYS56A (H-A distance 2.65 Å), LEU107A (H-A distance 2.54 Å), SER111A (H-A distance 2.15 Å), and ARG155A (two bonds with H-A distances of 2.27 Å and 2.67 Å). Donor angles ranged from 106.08° to 160.46°. Two salt bridges were identified between ARG155A and carboxylate groups of the ligand at distances of 3.71 Å and 4.71 Å. The combination of five hydrophobic contacts, six hydrogen bonds, and two salt bridges establishes moderate stabilization of the Hemidesmoside A-JAK1 complex at the nanomolar level.

3.2.3 Interaction between COX-2 and common phytocompounds from *Decalpis hamiltonii* and *Hemidesmus indicus*

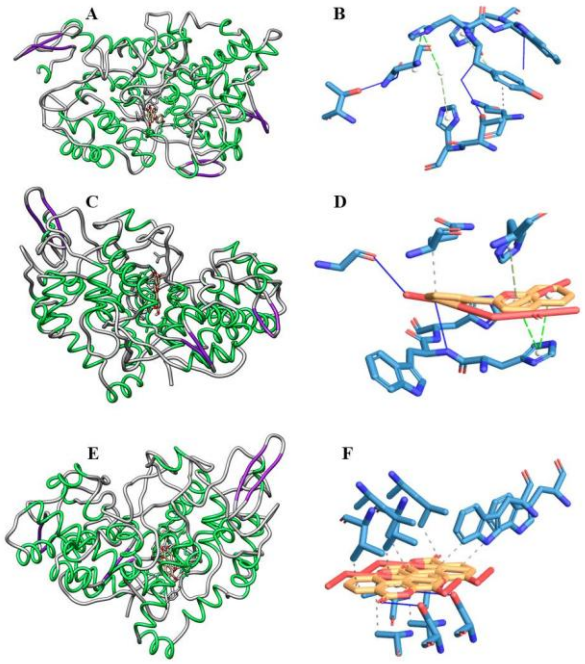


Figure 6. Molecular docking and interaction profiles of Kaempferol, quercetin and Ellagic acid with COX-2 (PDB: 5IKR). (A) Kaempferol with COX-2 (green helices, purple beta-sheets, white loops). (B) Kaempferol (orange sticks) in the binding pocket with interacting residues GLN171A, THR174A, THR180A, ASN350A, TYR353A, TRP355A, HIS175A, HIS354A, and HIS356A (cyan sticks). Interactions shown as dashed lines: hydrophobic (brown, 1 total), hydrogen bond (blue, 6 total), π-stacking (green, 4 total). Ki = 1.36 µM. (C) Quercetin with COX-2 (green helices, purple beta-sheets, white loops). (D) Quercetin (orange sticks) in the binding pocket with interacting residues GLN171A, ALA167A, TRP355A, HIS175A, HIS354A, and HIS356A (cyan sticks). Interactions shown as dashed lines: hydrophobic (brown, 1 total), hydrogen bond (blue, 2 total), π-stacking (green, 4 total),), Ki = 825 nM. (E) Ellagic acid with COX-2 (green helices, purple beta-sheets, white loops). (F) Ellagic acid (orange sticks) in the binding pocket with interacting residues VAL317A, LEU320A, TRP355A, VAL491A, ALA495A, and SER498A (cyan sticks). Interactions shown as dashed lines: hydrophobic (brown, 5 total), hydrogen bond (blue, 1 total), Ki = 3.76 µM.

During the COX-2 protein interaction, kaempferol and quercetin showed binding affinities of −8 kcal/mol and −8.3 kcal/mol, respectively, indicating favorable binding interactions. Quercetin formed one hydrophobic interaction with GLN-171, two hydrogen bonds with ALA-167 and TRP-355, and four π-stacking interactions with HIS-175, HIS-354, and HIS-356. Kaempferol formed six hydrogen bonds with amino acid residues, such as THR-174, THR-180, ASN-350, and TRP-355; one hydrophobic interaction with GLN-171; and four π-stacking interactions with HIS-175, HIS-354, and HIS-356. Ellagic acid showed a binding affinity of −7.4 kcal/mol against COX-2 through five hydrophobic interactions with VAL-317, LEU-320, TRP-355, VAL-491, and ALA-495, and one hydrogen bond with SER-498. However, 2-HMB and vanillin exhibit lower binding affinities of −5 kcal/mol and −6.2 kcal/mol, respectively, due to their smaller molecular sizes relative to the active site, resulting in weaker interactions.

Interaction between COX-2 and phytocompounds from *Hemidesmus indicus.*

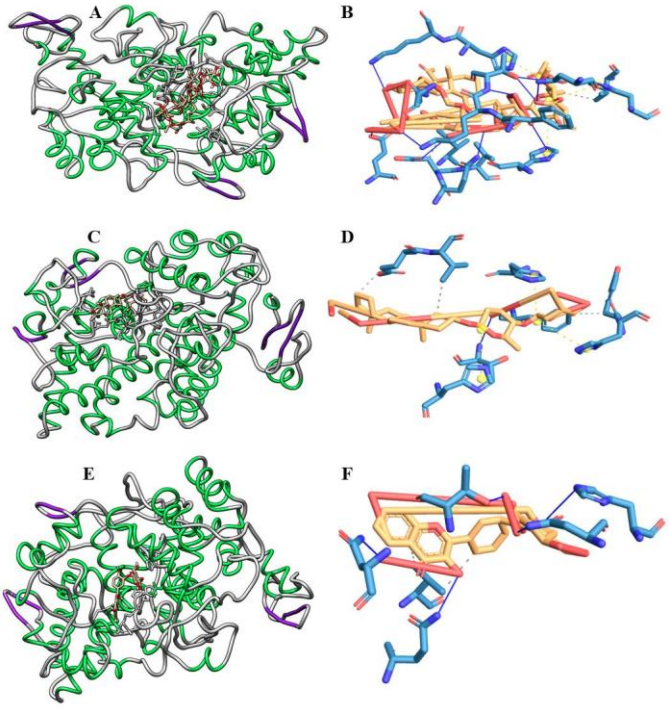


Figure 7. Molecular docking and interaction profiles of Hemidesmoside B, Heminine and Quercetin-O-glucoside with COX-2 (PDB: 5IKR). (A) Hemidesmoside B with COX-2 (green helices, purple beta-sheets, white loops). (B) Hemidesmoside B (orange sticks) in the binding pocket with interacting residues PHE178A, ILE242A, GLU258A, VAL259A, VAL415A, HIS175A, LYS179A, THR180A, LYS183A, ASN190A, GLU240A, GLN257A, and ASN350A (cyan sticks). Interactions shown as dashed lines: hydrophobic (brown, 5 total), hydrogen bond (blue, 12 total). Ki = 1.15 µM. (C) Heminine with COX-2 (green helices, purple beta-sheets, white loops). (D) Heminine (orange sticks) in the binding pocket with interacting residues PHE178A, GLU258A, VAL259A, TYR353A, THR180A, HIS175A, HIS182A, and HIS354A (cyan sticks). Interactions shown as dashed lines: hydrophobic (brown, 4 total), hydrogen bond (blue, 1 total), salt bridge (yellow, 3 total). Ki = 253 nM. (E) Quercetin-O-glucoside with COX-2 (green helices, purple beta-sheets, white loops). (F) Quercetin-O-glucoside (orange sticks) in the binding pocket with interacting residues VAL259A, THR180A, ASN190A, GLN257A, ASN350A, and HIS354A (cyan sticks). Interactions shown as dashed lines: hydrophobic (brown, 2 total), hydrogen bond (blue, 5 total). Ki = 354 nM.

HI exhibited stronger binding affinities and a greater number of noncovalent interactions compared to those from DH. During the COX-2 protein interaction, Hemidesmoside B, Heminine, and Quercetin-O-glucoside exhibited strong binding within the active site, with calculated inhibition constants (Ki) of 1.15 µM**,** 253 nM**,** and 354 nM**,** respectively. Hemidesmoside B formed five hydrophobic interactions with PHE178A, ILE242A, GLU258A, VAL259A, and VAL415A, together with 12 hydrogen bonds involving HIS175A, LYS179A, THR180A, LYS183A, ASN190A, GLU240A, GLN257A, ASN350A, and GLU258A, indicating stable binding within the COX-2 binding pocket. Heminine demonstrated the strongest interaction profile, forming four hydrophobic interactions with PHE178A, GLU258A, VAL259A, and TYR353A, one hydrogen bond with THR180A, and three salt bridges involving HIS175A, HIS182A, and HIS354A, which contributed to its lowest Ki value. Quercetin-O-glucoside also exhibited favorable binding, forming two hydrophobic interactions with VAL259A and HIS354A, along with five hydrogen bonds involving THR180A, ASN190A, GLN257A, ASN350A, and HIS354A. Overall, the phytocompounds from *Hemidesmus indicus* displayed stronger binding interactions and

more extensive noncovalent contacts with COX-2 than those identified from DH, suggesting that HI represents a more promising source of anti-inflammatory phytoconstituents targeting COX-2.

Table 2. *Summary of Molecular Docking Binding Energies of Selected Phytocompounds Against Inflammatory Targets*

Compound	**Caspase-1 (6F6R)**	**JAK-1 (6N77)**	**COX-2 (5IKR)**
2-Hydroxy-4-methoxybenzaldehyde (HMB)	-5.2	-5.6	-5.0
β-Amyrin	-5.6	-10.9	-2.5
Borneol	-5.5	-5.3	-4.2
β-Sitosterol	-	-8.7	-6.8
Kaempferol	-4	-8.6	-8.0
Ellagic acid	-	-	-7.4
Denicunine	—	-10.0	-2.4
Hemidesmoside A	—	-8.9	-6.9
Hemidesmoside B	—	-7.8	-8.1
Heminine	—	-9	-9.0
Quercetin-O-glucoside	—	-9.6	-8.8
Native Ligand (Redocking Control)	**-3.6**	**-8.5**	**-8.6**

Some of the phytocompounds were found to be effective binders of the target with the selectivities of β-Amyrin of −10.9 kcal/mol and Denicunine of −10.0 kcal/mol showing maximum probable binding compared to co-crystallized ligand of JAK-1 which showed −8.5 kcal/mol. Among the COX-2 enzyme, Heminine (−9.0 kcal/mol) and Quercetin-O-glucoside (−8.8 kcal/mol) showed binding energies that are similar to or better than the reference ligand i.e. mefenamic acid (−8.6 kcal/mol). On the other hand, the binding energies near Caspase-1 were not as strong, with β-Amyrin (−5.6 kcal/mol) and Borneol (−5.5 kcal/mol) having the best binding energies amongst the phytocompounds tried. From these results, it might be inferred that metabolites of Hemidesmus indicus are multi-targeted against inflammation as compared to common phytoconstituents as well as reference ligands.

Table 3. *Ranking of Top Phytocompounds Based on Predicted Binding Affinity Against Selected Inflammatory Targets*

Rank	**Caspase-1 (6F6R)**	**Binding Energy (kcal/mol)**
1	β-Amyrin	-5.6
2	Borneol	-5.5
3	2-Hydroxy-4-methoxybenzaldehyde (HMB)	-5.2

Rank	JAK-1 (6N77)	Binding Energy (kcal/mol)
1	β-Amyrin	-10.9
2	Denicunine	-10.0
3	Quercetin-O-glucoside	-9.6

Rank	COX-2 (5IKR)	Binding Energy (kcal/mol)
1	Heminine	-9.0
2	Quercetin-O-glucoside	-8.8
3	Hemidesmoside B	-8.1

The analysis of the interaction of the investigated phytocompounds showed that β-Amyrin showed the greatest binding energy during binding with both the Caspase-1 and JAK-1 (−5.6 kcal/mol and −10.9 kcal/mol respectively). Two unique metabolites, Denicunine and Hemidesmoside A were also found to show excellent affinity to the JAK-1 and hence their role in modulation of the cytokine mediated inflammatory signaling can be postulated. For COX-2, Heminine was the strongest predictor to interact (-9.0 kcal/mol), Quercetin-O-glucoside was nearly as strong predictor (-8.8 kcal/mol) and Hemidesmoside B was third in prediction of interaction (-8.1 kcal/mol). Interestingly, all the best COX-2 inhibitors were only found to be present in HI thus substantiating the theory that this species has more anti-inflammatory metabolites as compared to DH.

3.3 *In Silico* Prediction of Pharmacokinetic Properties

The ADMET profiles of the seven selected compounds, predicted using pkCSM, together with a cross-validation of their CYP450 inhibition potential using SwissADME, are summarised in Tables 4–8.

Absorption

Table 4. In silico absorption characteristics of selected compounds

Compounds	Water solubility (log mol/L)	HIA	Skin permeability (log Kp)	P-glycoprotein substrate
2-Hydroxy-4-methoxybenzaldehyde	−1.60	Absorbed	−2.50	Non-substrate
Borneol	−2.51	Absorbed	−2.73	Non-substrate
β-Sitosterol	−7.90	Absorbed	−2.91	Non-substrate
Ellagic acid	−4.36	Absorbed	−0.72	Non-substrate
Kaempferol	−3.33	Absorbed	−0.35	Non-substrate
Quercetin	−3.33	Non-absorbed	1.27	Substrate

The analyzed compounds exhibited aqueous solubility values ranging from −1.60 to −7.90 log mol/L, with 2-hydroxy-4-methoxybenzaldehyde being the most water-soluble and β-sitosterol the least soluble, reflecting the highly lipophilic steroidal structure. Among the extracted phytocompounds, such as 2-hydroxy-4-methoxybenzaldehyde, borneol, β-sitosterol, ellagic acid, and kaempferol, were predicted to be well absorbed from the human intestine, whereas quercetin was predicted to be non-absorbed. Skin permeability (log Kp) values were more negative (indicating lower dermal permeability) for the terpenoid and steroidal compounds (borneol, −2.73; β-sitosterol, 2.91) than for the phenolic compounds ellagic acid, kaempferol, and quercetin (−0.72, −0.35, and 1.27, respectively), the latter indicating comparatively greater potential for skin penetration. Quercetin was the only compound predicted to be a P-glycoprotein substrate, suggesting it may be subject to efflux-mediated transport, which could limit its systemic exposure; the remaining compounds were predicted to be non-substrates.

Distribution

Table 5. In silico distribution characteristics of selected compounds

Compounds	VDss (human) (log L/kg)	BBB permeability (log BB)
2-Hydroxy-4-methoxybenzaldehyde	1.33	−2.42
Borneol	1.19	−2.54
β-Sitosterol	1.62	−2.12
Ellagic acid	0.56	−2.85
Kaempferol	0.27	−2.75
Quercetin	0.87	−4.19

The predicted steady-state volume of distribution (VDss) ranged from 0.27 to 1.62 log L/kg, with the highest value indicating relatively extensive distribution into tissues rather than remaining confined to plasma. β-Sitosterol (1.62), 2-hydroxy-4-methoxybenzaldehyde (1.33), and borneol (1.19) showed the highest values, while kaempferol showed the lowest VDss (0.27). All six compounds exhibited negative log BB values (ranging from −2.12 to 4.19), with quercetin showing the most negative value (−4.19), indicating poor predicted penetration of the blood–brain barrier and the most restricted CNS distribution among the set.

Metabolism

Table 6. In silico metabolism characteristics of selected compounds

Compounds	CYP2D6 substrate	CYP3A4 substrate	CYP1A2 inhibitor	CYP2C19 inhibitor	CYP2C9 inhibitor	CYP2D6 inhibitor	CYP3A4 inhibitor
2-Hydroxy-4-	Non-	Non-	Non-	Non-	Non-	Non-	Non-

methoxybenzaldehyde	substrate	substrate	inhibitor	inhibitor	inhibitor	inhibitor	inhibitor
Borneol	Substrate	Non-substrate	Non-inhibitor	Non-inhibitor	Non-inhibitor	Non-inhibitor	Non-inhibitor
β-Sitosterol	Non-substrate	Substrate	Non-inhibitor	Non-inhibitor	Non-inhibitor	Non-inhibitor	Non-inhibitor
Ellagic acid	Non-substrate	Non-substrate	Inhibitor	Inhibitor	Non-inhibitor	Non-inhibitor	Non-inhibitor
Kaempferol	Non-substrate	Non-substrate	Inhibitor	Non-inhibitor	Inhibitor	Non-inhibitor	Inhibitor
Quercetin	Non-substrate	Non-substrate	Non-inhibitor	Non-inhibitor	Non-inhibitor	Non-inhibitor	Non-inhibitor

Among the six evaluable compounds, borneol was the only predicted CYP2D6 substrate and β-sitosterol the only predicted CYP3A4 substrate; none of the remaining compounds were predicted as substrates of either isoform. With respect to CYP450 inhibition, ellagic acid was predicted to inhibit CYP1A2 and CYP2C19, while kaempferol was predicted to inhibit CYP1A2, CYP2C9 and CYP3A4. The remaining compounds, including 2-hydroxy-4-methoxybenzaldehyde, borneol, β-sitosterol and quercetin, were not predicted to inhibit any of the five CYP450 isoforms assessed by pkCSM.

Table 7. SwissADME CYP inhibition results

Compound	CYP1A2 inhibitor	CYP2C19 inhibitor	CYP2C9 inhibitor	CYP2D6 inhibitor	CYP3A4 inhibitor
2-Hydroxy-4-methoxybenzaldehyde	No	No	No	No	No
Borneol	No	No	No	No	No
β-Sitosterol	No	No	No	No	No
Ellagic acid	Yes	No	No	No	No
Kaempferol	Yes	No	No	Yes	Yes
Quercetin	Yes	No	No	Yes	Yes
β-Amyrin	No	No	No	No	No

Cross-validation with SwissADME showed general agreement with the pkCSM predictions for 2-hydroxy-4-methoxybenzaldehyde, borneol and β-sitosterol, all of which were predicted as non-inhibitors of the five CYP450 isoforms by both platforms. Ellagic acid was consistently predicted to inhibit CYP1A2 by both servers, although SwissADME did not flag it as a CYP2C19 inhibitor as pkCSM had. Notable discrepancies were observed for kaempferol and quercetin: SwissADME additionally predicted both compounds as inhibitors of CYP2D6 and CYP3A4, and identified quercetin as a CYP1A2 inhibitor — interactions that were not flagged by pkCSM. β-Amyrin, for which pkCSM

returned no prediction, was classified as a non-inhibitor of all five isoforms by SwissADME. These differences reflect the distinct algorithms and training datasets underlying the two platforms and highlight the value of cross-validating CYP450 inhibition predictions using more than one in silico tool.

Excretion

Table 7. In silico excretion characteristics of selected compounds

Compounds	Total Clearance (log mL/min/kg)	Renal OCT2 inhibitor
2-Hydroxy-4-methoxybenzaldehyde	7.56	Non-inhibitor
Borneol	11.70	Non-inhibitor
β-Sitosterol	10.95	Non-inhibitor
Ellagic acid	7.70	Non-inhibitor
Kaempferol	5.81	Non-inhibitor
Quercetin	13.32	Non-inhibitor

Predicted total clearance values ranged from 5.81 to 13.32 log mL/min/kg. Quercetin showed the highest predicted clearance (13.32), followed by borneol (11.70) and β-sitosterol (10.95), suggesting comparatively rapid elimination from systemic circulation, while kaempferol showed the lowest clearance (5.81). None of the evaluable compounds were predicted to inhibit the renal organic cation transporter 2 (OCT2), indicating a low likelihood of OCT2-mediated renal drug–drug interactions or impaired renal excretion for this compound set.

Toxicity

Table 8. In silico toxicity predictions for selected compounds

Compounds	AMES toxicity	MTD (human) (log mg/kg/day)	Oral rat acute toxicity (LD50) (mol/kg)	Oral rat chronic toxicity (LOAEL) (log mg/kg_bw/day)	Hepato-toxicity	Skin sensitisation
2-Hydroxy-4-methoxybenzaldehyde	Safe	1.06	1.95	1.91	Safe	Toxic
Borneol	Safe	0.55	1.66	1.32	Safe	Toxic
β-Sitosterol	Safe	2.07	2.19	1.92	Safe	Toxic
Ellagic acid	Safe	1.14	2.31	3.40	Toxic	Toxic
Kaempferol	Safe	1.17	2.46	3.03	Toxic	Toxic
Quercetin	Toxic	0.85	2.46	4.11	Safe	Toxic

Quercetin was the only compound predicted to be AMES-positive, indicating potential mutagenic risk, while the remaining six compounds were predicted to be non-mutagenic (safe). Predicted maximum tolerated dose (MTD) in humans ranged from 0.55 to 2.07 log mg/kg/day, with β-sitosterol showing the

highest tolerated dose and borneol the lowest. Oral rat acute toxicity (LD50) values ranged from 1.66 to 2.46 mol/kg, and oral rat chronic toxicity (LOAEL) values ranged from 1.32 to 4.11 log mg/kg_bw/day, with quercetin showing the highest LOAEL value among the set. Ellagic acid and kaempferol were predicted to be hepatotoxic, whereas the remaining compounds were predicted as safe with respect to hepatotoxicity. Notably, all seven compounds, including β-amyrin, were predicted to be positive for skin sensitisation, indicating a shared potential to provoke dermal sensitisation reactions that should be taken into account for any topical application of these compounds.

4. Discussion

4.1 Traditional Substitutability of HI and DH

Ayurvedic and ethnomedicinal formulations often use HI and DH interchangeably because they share similar aromatic and therapeutic properties, despite their differing phytochemical profiles (Fang, Z., 2013). Pharmacognostic and phytochemical investigations of both species reveal several shared compounds—particularly 2-hydroxy-4-methoxy benzaldehyde (2H4MB)—which support their practical substitution (Shendge, P. N. (2020). This study examines whether the phytocompounds from both species interact similarly with key inflammatory targets involved in skin inflammation, building on these findings.

LC–MS data indicate that, although both species share phytochemical classes, their overall metabolite profiles are distinct. Phenolic acids, flavonoids, steroids, and triterpenoids characterize DH, while glycosides, saponins, pregnane derivatives, and alkaloids are prominent in HI. Common phytochemicals likely account for their similar medicinal uses, whereas unique compounds provide species-specific pharmacological effects and organ selectivity (Jadhav, S., (2024).

4.2 Validation of the Molecular Docking Workflow

Molecular docking predictions rely on accurately reproducing ligand–protein interactions observed in experiments. To validate the docking procedure, we docked co-crystallized ligands belonging to Caspase -1 (6F6R), JAK-1 (6N77), and COX-2 (5IKR). All redocked ligand conformers matched their crystallographic structures, with an RMSD of 0.0 Å, demonstrating the feasibility of the docking parameters and active site definitions in this study. We used the binding energies of the Caspase-1 ligand (−3.6 kcal/mol), JAK-1 inhibitor (−8.5 kcal/mol), and mefenamic acid (−8.6 kcal/mol) bound to COX-2 as controls for the binding energies observed between phytocompounds. These results clarify and bolster confidence in the reliability of the protein–ligand interactions predicted by the software, and their interpretation assists in docking analyses.

4.2.1 Caspase-1 Inhibition and Inflammasome Modulation

Caspase-1 has been suggested to be involved in a number of inflammatory skin diseases, as a consequence of its excessive activation, and is therefore a therapeutic target (Fenini, G., (2023;

Sollberger, G., (2014). It plays a key role in the maturation and secretion of pro-inflammatory cytokines, such as Interleukin-1β and Interleukin-18 (Burian, M. (2023). A list of the compounds studied in this research indicates that the most favorable binders to Caspase-1 were β-amyrin, borneol, and 2H4MB, with binding energies of −5.6, −5.5,, and −5.2 kcal/mol, respectively.

Upon docking, these compounds were found to engage in several nonpolar and hydrogen-bond interactions within the active-site domain, which assisted in the proper stabilization of the ligand. The binding energies of these phytocompounds were surprisingly more than the redocked native ligand, suggesting that these phytocompounds may be interesting inhibitors, with the most promising compound being beta-amyrin with a good docking score via extensive hydrogen-bonding and hydrophobic network substructures. The results support previous reports on the anti-inflammatory activity of herbal medicines containing triterpenoids and terpenoids and suggest that these molecules may be responsible for the anti-inflammatory effects of both HI and DH.

4.2.2Modulation of JAK-1 Signaling by Phytocompounds

The JAK/STAT signaling pathway is one of the important intracellular pathways involved in inflammatory cytokine responses in the skin. JAK-1 signaling defects are associated with chronic inflammatory skin diseases, such as psoriasis, atopic dermatitis, and autoimmune diseases (Bao, L., (2013). Thus, inhibition of JAK-1 appears as a good therapeutic option.

Similar analysis for all the targets showed that Hemidesmoside A (−8.9 kcal/mol), Denicunine (−10.0 kcal/mol), and β-Amyrin (−10.9 kcal/mol) had the highest affinity for JAK-1. The values were more favorable than (−8.5 kcal/mol) for the co-crystallized JAK-1 inhibitor, showing very attractive binding inside the ATP-binding cavity. The high number of hydrogen bonds and hydrophobic contacts seen for these compounds provides evidence of a high degree of geometric complementarity in the active site.

Interestingly, Denicunine and Hemidesmoside A are metabolites detected only in HI. Due to their high binding affinity for JAK-1, they may have a wide range of abilities to inhibit inflammatory signaling via cytokines beyond DH. The findings indicate a molecular mechanism for the anti-inflammatory efficacy of HI with a a multitarget profile, as illustrated,, and emphasize the need for species-specific phytochemicals for therapeutic efficacy.

4.2.3 COX-2 Inhibition and Anti-inflammatory Potential

The initial step in the inflammatory process is the conversion of arachidonic acid to prostaglandins, which are responsible for inflammation, pain, edema, and vascular permeability; this is catalyzed by the central enzyme cyclooxygenase-2 (COX-2) (Simard, M., & Thivierge, M. (2022). Its selective Inhibition is one of the most important therapeutic targets to control inflammatory disorders.

In the present study, it was found that the COX-2 enzyme has high predicted binding interactions with some of the phytocompounds extracted from HI. The binding affinity of Heminine (–9.0 kcal/mol), Quercetin-O-glucoside (–8.8 kcal/mol), and Hemidesmoside B (–8.1 kcal/mol) was found to be

maximum, in this order. On the other hand, the values of binding energies of Heminine and Quercetin-O-glucoside were similar to or slightly higher than that of the reference ligand mefenamic acid (−8.6 kcal/mol).

Detailed interaction analysis revealed many interactions, including hydrogen bonding, hydrophobic contacts, and salt-bridge interactions, between the catalytic channel of COX-2 and the drug. These interactions are important for properly orienting the ligands in the active site, positioning them, and preventing other groups of the substrate from reaching the catalytic residues. In addition, the more complex COX-2-interacting metabolic patterns among HI-specific metabolites will provide further evidence that HI may have a more far-reaching anti-inflammatory effect, involving modulation of all inflammatory pathways.

4.3 Comparison with Native Ligands

On the other hand, revealed that the native ligand beta-Amyrin could be redocked into this ATP-binding pocket, with a binding affinity of −10.9 kcal/mol, whereas the co-crystallized inhibitor bound with −8.5 kcal/mol. Likewise, Denicunine has shown a binding affinity of -10.0 kcal/mol, thereby further supporting its role as a JAK-1 modulator.

Heminine had a binding energy of −9.0 kcal/mol as compared to the −8.6 kcal/mol as observed for mefenamic acid, while Quercetin-O-glucoside has a similar energy of binding equal to −8.8 kcal/mol. Based on these observations, it can be inferred that several natural phytocompounds exhibit an interaction profile similar to that of known anti-inflammatory ligands. Such comparisons, although they might not define the pharmacological activity per se, do offer useful evidence of the therapeutic potential of these metabolites in docking energies.

4.4 Consequences of Traditional Medicine and the Outlook for the Future

The results of the present work provide, at the molecular level, confirmation of the traditional use of HI and DH in medicines. The common phytocompounds 2H4MB and the fact that they are both historically and ethnomedically interchangeable support this. However, identification of several HI-specific metabolites that interacted more strongly with both JAK-1 and COX-2 suggests that, at times, it may not be possible to achieve the full therapeutic effect through replacement.

It has implications for the standardization, quality assurance, and conservation of these herbs. DH can be used as a legitimate functional counterpart to HI-based formulations,, which primarily utilize common metabolites, but some therapeutic activity is likely to be based on the exclusive phytochemical constituents of HI.

4.5 In Silico Prediction of Pharmacokinetic Properties

In silico ADMET profiling provides a preliminary indication of the pharmacokinetic and safety profiles of the prospective drug candidates (Kar, S., 2020). In the present study, seven phytocompounds were tested to predict oral absorption, limited central nervous system (CNS) penetration, and a relatively low

risk of major cytochrome P450–mediated drug–drug interactions. The oral absorption model predicted that 2-hydroxy-4-methoxybenzaldehyde, borneol, β-sitosterol, ellagic acid, and kaempferol would be well absorbed, with aqueous solubility values ranging from −1.60 to −7.90 log mol/L. the polar structures are dispersible in aqueous media, whereas bulky structures like β-sitosterol are poorly soluble owing to lipophilicity (Veber, D. F., 2002). Quercetin was predicted to be poorly absorbed and a P-glycoprotein substrate, indicating limited systemic exposure, with reduced oral bioavailability (Song, Q., 2026). Phenolic compounds were also predicted to have higher skin permeability than terpenoid and steroidal molecules, indicating greater suitability for topical delivery.

Distribution predictions show steady-state moderate-to-high distribution volumes, especially for β-sitosterol, 2-hydroxy-4-methoxybenzaldehyde, and borneol, which suggest high tissue partitioning, long duration of action, and dosing implications. Kaempferol has the lowest VDss and is expected to stay more concentrated in plasma (Pires, D. E., Blundell, T. L., & Ascher, D. B., 2015). All compounds have negative log BB values, with quercetin being the most negative, indicating limited blood–brain barrier penetration and a low probability of CNS effects, thereby limiting their use in CNS-targeting therapies (Daina et al., 2017).

Borneol and β-sitosterol are predicted substrates of CYP2D6 and CYP3A4, indicating their clearance may be influenced by structural differences or co-medication at these pathways (Xiong et al., 2021; Zanger & Schwab, 2013). pkCSM predicted no inhibition of the investigated CYP isoforms for 2-hydroxy-4-methoxybenzaldehyde, borneol, β-sitosterol, or quercetin, while ellagic acid and kaempferol showed inhibitory potential against multiple isoforms, indicating a higher risk of metabolic interactions (Pires et al., 2015). Cross-validation with SwissADME confirmed the low inhibition risk for 2-hydroxy-4-methoxybenzaldehyde, borneol, and β-sitosterol, and consistently identified ellagic acid as a CYP1A2 inhibitor (Azzam, 2023). Predicted total clearance values varied widely, with quercetin, borneol, and β-sitosterol showing higher clearance, suggesting rapid elimination and potentially shorter dosing intervals, while kaempferol may persist longer.

Toxicity predictions showed that quercetin was the only AMES-positive compound, indicating a possible mutagenic risk and the need for toxicological evaluation. This aligns with reports that some flavonoids can have pro-oxidant or DNA-damaging effects under certain conditions (Xiong et al., 2021). Ellagic acid and kaempferol were predicted to be hepatotoxic, while 2-hydroxy-4-methoxybenzaldehyde, borneol, β-sitosterol, and quercetin were considered non-hepatotoxic within model limits.

4.6 Limitations of the Study

The present investigations have mainly been carried out through molecular Docking simulations and phytochemical profiling. Molecular docking is a static approach to representing protein–ligand

interaction, and although the docking protocol was validated by redocking studies, all protein-ligand conformations cannot be well captured in molecular docking. In molecular dynamics, Free energies and validation by biological experiments were performed. Further, only a few of the identified phytocompounds were studied, as determined by LC-MS. The reported binding affinities are therefore only indicative of target engagement, not of biological efficacy. In the future, studies combining computation dynamics and invitro studies should be conducted to validate the therapeutic potential of the identified compounds.

5. Conclusion

The present study performed a comparative in silico analysis of the phytocompounds from HI and DH against inflammatory targets involved in skin inflammation, namely Caspase-1, JAK-1 and COX-2. LC–MS-based phytochemical profiling revealed both shared and species-specific compound classes, which were shown by molecular docking to bind multiple inflammatory proteins. Redocking of the co-crystallised ligands gave acceptable results, supporting the validity of the computational workflow.

Both species showed predicted multitarget anti-inflammatory potential through interactions with proteins involved in inflammasome activation, cytokine signalling and prostaglandin biosynthesis. The presence of common phytocompounds, particularly 2-hydroxy-4-methoxybenzaldehyde, offers a molecular explanation for the traditional interchangeability of the two species. However, several metabolites identified in HI, namely denicunine, hemidesmosides, heminine and quercetin-O-glucoside, showed higher average predicted binding affinities and more non-covalent interactions than the phytocompounds identified from DH.

Comparison with native ligands showed that some metabolites had binding energies comparable to those of the native ligands, particularly for COX-2 and JAK-1. These findings suggest that traditional substitution is plausible because shared bioactive compounds are present. However, HI contains a broader range of compounds that may engage multiple inflammatory pathways.

In conclusion, both species showed predicted multitarget anti-inflammatory activity. Although the two plants share common phytocompounds, the unique metabolites of HI had higher predicted affinities, which suggests they may contribute substantially to its anti-inflammatory activity. Further studies, including molecular dynamics simulations and experimental validation, are needed to confirm these findings and establish their therapeutic value and biological relevance.

Data availability

The LC-MS profiling data of Hemidesmus indicus and Decalepis hamiltonii generated and analysed during this study are openly available in the Zenodo repository at https://doi.org/10.5281/zenodo.23610566. All other data supporting the findings of this study are included within the article and its supplementary materials.

6. References

1. Ahmad Z, Shahzad A, Emamverdian A, Ramakrishnan M, Ding Y (2022) Genus Decalepis: biology, importance and biotechnological interventions. Agronomy 12:855. https://doi.org/10.3390/agronomy12040855

2. Aswathanarayan JB, Vittal RR (2022) Plant-derived natural products for drug discovery: current approaches and prospects. Biomed Pharmacother 156:113954. https://doi.org/10.1016/j.biopha.2022.113954

3. Azzam KA (2023) SwissADME and pkCSM webservers predictors: an integrated online platform for accurate and comprehensive predictions for in silico ADME/T properties of artemisinin and its derivatives. Kompleksnoe Ispolzovanie Mineralnogo Syra = Complex Use of Mineral Resources 325:14–21

4. Bao L, Zhang H, Chan LS (2013) The involvement of the JAK-STAT signaling pathway in chronic inflammatory skin disease atopic dermatitis. JAK-STAT 2:e24137. https://doi.org/10.4161/jkst.24137

5. Burian M, Schmidt MF, Yazdi AS (2023) The NLRP1 inflammasome in skin diseases. Front Immunol 14:1111611. https://doi.org/10.3389/fimmu.2023.1111611

6. Cui L, Liu P, Wu K, Han X, Peng G (2026) Targeting the JAK/STAT pathway in atopic dermatitis. Front Immunol 17:1757562. https://doi.org/10.3389/fimmu.2026.1757562

7. Daina A, Michielin O, Zoete V (2017) SwissADME: a free web tool to evaluate pharmacokinetics, drug-likeness and medicinal chemistry friendliness of small molecules. Sci Rep 7:42717

8. Das S, Bisht SS (2013) The bioactive and therapeutic potential of Hemidesmus indicus R. Br. (Indian sarsaparilla) root. Phytother Res 27:791–801. https://doi.org/10.1002/ptr.4788

9. Ekor M (2014) The growing use of herbal medicines: issues relating to adverse reactions and challenges in monitoring safety. Front Pharmacol 4:177. https://doi.org/10.3389/fphar.2013.00177

10. Fang Z, Zhang M, Yi Z, Wen C, Qian M, Shi T (2013) Replacements of rare herbs and simplifications of traditional Chinese medicine formulae based on attribute similarities and pathway enrichment analysis. Evid Based Complement Alternat Med 2013:136732. https://doi.org/10.1155/2013/136732

11. Fenini G, Karakaya T, Hennig P, Di Filippo M, Beer H-D (2020) The NLRP1 inflammasome in human skin and beyond. Int J Mol Sci 21:4788. https://doi.org/10.3390/ijms21134788

12. Guo H, Callaway JB, Ting JPY (2015) Inflammasomes: mechanism of action, role in disease, and therapeutics. Nat Med 21:677–687. https://doi.org/10.1038/nm.3893

13. Hao D-C, Wang Y-X, He C-N, Spjut RW (2023) Editorial: plant-derived natural compounds in drug discovery: the prism perspective between plant phylogeny, chemical composition, and medicinal efficacy, volume II. Front Plant Sci 14:1324514. https://doi.org/10.3389/fpls.2023.1324514

14. Jadhav S, Jagtap S, Zanwar A, Singh EA (2024) A comparative analysis of four ‘Sariva’ plants: HPTLC profiling and antioxidant activity. Ecol Environ Conserv 30:S55–S63

15. Kar S, Leszczynski J (2020) Open access in silico tools to predict the ADMET profiling of drug candidates. Expert Opin Drug Discov 15:1473–1487

16. Kharat TD, Mokat DN (2021) Comparative study of essential oil found in roots of wild and cultivated drug Anantmool. J Essent Oil Bear Plants 24:1227–1234. https://doi.org/10.1080/0972060X.2022.2026257

17. Kulatunge DR, Jayawardana KH, Abeysekera AM, Wijeyaratne SC, Gunaherath GKB (2025) In vitro cell migration enhancing constituents from Decalepis hamiltonii, a plant used in the preparation of Pinda oil, a medicinal oil used in Ayurveda for wound management. Nat Prod Res 39:2990–2996. https://doi.org/10.1080/14786419.2024.2305220

18. Lakshman K, Yoganarasimhan SN, Shivaprasad HN, Jaiprakash B, Mohan S (2006) Anti-inflammatory and antipyretic activity of Decalepis hamiltonii root extract. Pharm Biol 44:127–129. https://doi.org/10.1080/13880200600592269

19. Naik Y, Jayaram S, Nayaka MH, Dharmesh SM (2007) Gastroprotective effect of swallow root (Decalepis hamiltonii) extract: possible involvement of H+-K+-ATPase inhibition and antioxidative mechanism. J Ethnopharmacol 112:173–179. https://doi.org/10.1016/j.jep.2007.02.019

20. Pathan JK, Gautam G, Gupta AK (2018) Investigation of anti-inflammatory activity of Hemidesmus indicus L. on carrageenan-induced paw oedema in rats. J Drug Deliv Ther 8:492–494. https://doi.org/10.22270/jddt.v8i5.1912

21. Pires DE, Blundell TL, Ascher DB (2015) pkCSM: predicting small-molecule pharmacokinetic and toxicity properties using graph-based signatures. J Med Chem 58:4066–4072

22. Ren Q, Qu L, Yuan Y, Wang F (2024) Natural modulators of key signaling pathways in skin inflammageing. Clin Cosmet Investig Dermatol 17:2967–2988. https://doi.org/10.2147/CCID.S477232

23. Swati S, Justin A, Palanisamy DS, Sivasankaran P (2020) Evaluation of neuroprotective potential of methanolic extract of Hemidesmus indicus extract in Aβ (1-42) induced rats. Int J Res Pharm Sci 11:7495–7502

24. Shendge PN, Patil SB (2020) Pharmacognostic and phytochemical studies on Hemidesmus indicus and its substitute Decalepis hamiltonii – a review. Int J Bot Stud 5:224–231

25. Sollberger G, Strittmatter GE, Grossi S, Beer HD (2014) Caspase-1: the inflammasome and beyond. Innate Immun 20:115–125. https://doi.org/10.1177/1753425913484374

26. Song Q, Liu L, Yang Q, Pan M, Zhang Y (2026) Quercetin in metabolic diseases: mechanisms, therapeutics, and multidimensional frontiers. Front Endocrinol 17:1800322

27. Sujith T, Susikumar S, Sunilkumar KN, Radha P, Shakila R, Gopinath P (2021) Detection of adulteration of Decalepis hamiltonii Wight & Arn. with Hemidesmus indicus (L.) R. Br. by pharmacognostic, molecular DNA fingerprinting by RAPD, chemical and HPTLC studies. Plant Sci Today 8:610–620. https://doi.org/10.14719/pst.2021.8.3.1151

28. Veber DF, Johnson SR, Cheng HY, Smith BR, Ward KW, Kopple KD (2002) Molecular properties that influence the oral bioavailability of drug candidates. J Med Chem 45:2615–2623

29. World Health Organization (2013) WHO traditional medicine strategy 2014–2023. World Health Organization, Geneva. Available at: https://www.who.int/publications/i/item/9789241506090

30. Xiong, G., Wu, Z., Yi, J., Fu, L., Yang, Z., Hsieh, C., Yin, M., Zeng, X., Wu, C., Lu, A. and Chen, X. (2021) ADMETlab 2.0: an integrated online platform for accurate and comprehensive predictions of ADMET properties. Nucleic Acids Res 49:W5–W14.

31. Zanger UM, Schwab M (2013) Cytochrome P450 enzymes in drug metabolism: regulation of expression, enzyme activities, and impact of genetic variation. Pharmacol Ther 138:103–141

Author contribution

Manisha performed the LC-MS/MS data screening, *in silico* molecular docking, Protein-Ligand Interaction Profiler (PLIP) analysis, ADMET reports, data visualization, and contributed significantly to both the initial draft and final manuscript preparation. Both authors read and approved the final version.

Reshma supervised the project, provided resources, funding, validated the computational results, and critically revised the final manuscript. Both authors read and approved the final version.

Funding:

This study was supported by the **Indian Council of Medical Research (ICMR)**, New Delhi, India, under the Indian ICMR Research Project grant **[Project ID: IIRP 2023-2084]** awarded to **Reshma**.

Acknowledgements:

The authors gratefully acknowledge the **Central Research Facility (CRF) at the National Institute of Technology Karnataka (NITK), Surathkal**, for providing the LC-MS/MS analytical instrumentation facilities. The authors also acknowledge **Mr. Shashank Bhat** for his technical assistance in the extraction and preparation of crude plant samples. The authors also acknowledge **Dr. Keshava Chandra K**. M.Sc. Ph.D., Lecturer, Member Tree Authority, Moodubidri Forest Range (A6/CR-10/ Authority Formation) and Life Member IAAT & IBC for his assistance with plant identification and taxonomic authentication.

Disclosure of AI usage

During the preparation of this manuscript, the authors used QuillBot, Grammarly, and Paperpal to assist with language improvement, including grammar correction, sentence clarity, and paraphrasing. All outputs were reviewed, verified, and integrated by the authors to ensure the manuscript reflects their expertise, voice, and originality. The authors take full responsibility for all content presented herein.

Supplementary Files

This is a list of supplementary files associated with this preprint. Click to download.

- supplimentory.docx